JGR Space Physics

RESEARCH ARTICLE
10.1029/2021JA030134

Key Points:

- The reconnection rate depends significantly on the properties of the diffusion region
- Even for very strong resistivities and varying shapes of the resistive region there exists a maximum rate that the system can support
- We show how the properties of the diffusion region are altered for various resistive spot magnitudes and shapes

Correspondence to:
J. Pérez-Coll Jiménez,
juditpcj@kth.se

Citation:
Pérez-Coll Jiménez, J., Tenfjord, P., Hesse, M., Norgren, C., Kwagala, N., Kolstø, H. M., & Spinnangr, S. F. (2022). The role of resistivity on the efficiency of magnetic reconnection in MHD. *Journal of Geophysical Research: Space Physics*, *127*, e2021JA030134. https://doi.org/10.1029/2021JA030134

Received 16 NOV 2021
Accepted 30 APR 2022

The Role of Resistivity on the Efficiency of Magnetic Reconnection in MHD

Judit Pérez-Coll Jiménez[1], Paul Tenfjord[1], Michael Hesse[2], Cecilia Norgren[1], Norah Kwagala[1], Håkon Midthun Kolstø[1], and Susanne Flø Spinnangr[1]

[1]Space Plasma Physics Group, University of Bergen, Bergen, Norway, [2]NASA Ames Research Center, Mountain View, CA, USA

Abstract Using a resistive MagnetoHydroDynamic (MHD) simulation, we study how the magnitude and shape of diffusion influence magnetic reconnection. Specifically, we investigate how and why the reconnection rate is influenced by variations in the diffusion distribution and magnitude. By running multiple MHD simulations where we vary the localized resistivity, we find that the properties of the diffusion region greatly influence the rate of reconnection. Increasing the magnitude of the imposed resistivity results in a higher reconnection rate, but the rate saturates at approximately 0.2. We show how a redistribution of the current density, leading to a bifurcated current sheet, play a major role in this limitation. In addition, we investigate the impact of different shapes of resistive region. The shape of the diffusion region also plays a major role in how efficient the reconnection energy conversion can operate. The highest reconnection rate, approximately 0.25, is achieved for an optimal opening angle. Our results imply that reconnection has a speed limit that may depend on properties outside the diffusion region.

Plain Language Summary Magnetic reconnection is a fundamental plasma process, which can explosively convert magnetic energy to particle energy. When reconnection operates, it releases almost all of the energy stored in the magnetic field to plasma acceleration and heating. The consequences of reconnection depend on the magnetic energy available and the process' ability to rapidly release the energy. Thus, the effectiveness of reconnection, which can be quantified by the rate at which energy is converted, is a key factor in understanding the consequences and implications of this universal process. This paper investigates how the reconnection rate depends on the resistivity in the system. In our fluid-based scheme, resistivity determines the plasma's ability to diffuse across the magnetic field - allowing new magnetic topologies to form. We show that, even when inserting very strong resistive spots with varying shapes, there appears to be a maximum rate of reconnection the system can support. In addition, we find that a sub-optimal choice of resistivity magnitude or shape of the resistive spot leads to lower overall reconnection rates. These results imply that the reconnection rate depends significantly on properties of the diffusion region, even if the size of that region is much smaller than the system.

1. Introduction

Magnetic reconnection is a universal process that converts magnetic energy to particle energy by changing the magnetic field topology. It is considered responsible for many plasma phenomena exhibiting particle acceleration and heating, and large magnetic geometry changes, such as stellar flares (Masuda et al., 1994; Shibata & Magara, 2011), magnetospheric substorms (Angelopoulos et al., 2008) and other high energy processes in astrophysical and laboratory systems (Sironi et al., 2015; Zweibel & Yamada, 2009). Thus, understanding the efficiency of magnetic reconnection is a key aspect of determining the consequence and impact of many phenomena and processes.

The simplest way of describing magnetic reconnection is given by the model developed by Sweet (1958) and Parker (1957). This model, which consists of a very elongated diffusion region, results in a reconnection rate too slow to explain the energy release time scales of flares and substorms (Parker, 1963, 1973). Petschek (1964) developed a new model which included a localized diffusion region with an open geometry, which could support much higher reconnection rates. Today, both numerical simulations and observations (Genestreti et al., 2018) suggest that the global rate of magnetic reconnection is $\simeq \mathcal{O}(0.1)$ in normalized units (Cassak et al., 2017), but the reason why reconnection is limited to this rate is still not completely understood (Liu et al., 2017).

Over the years, significant work has been done on the different mechanisms that influence the reconnection rate (Drake et al., 1994; Li & Liu, 2021; Liu et al., 2019). Recently, the importance of multi-species plasma on the efficiency of magnetic reconnection has been recognized in the community (e.g., Tenfjord et al., 2019; Toledo-Redondo et al., 2021). These plasma descriptions can be reproduced by models such as Particle-In-Cell (PIC) simulations. The present study uses a resistive MagnetoHydroDynamic (MHD) model to investigate what limits the effectiveness of magnetic reconnection. The benefit of resistive MHD is that we can control the magnitude and shape of the diffusion. This enables us to study how the process behaves and resolves different scenarios, for specific diffusion region properties.

The influence of the resistivity profile on the magnetic reconnection process has long been studied by various authors. Ugai and Tsuda (1977) obtained a stable Petschek open geometry in 2D MHD simulations with a localized resistivity at the x-line. To mimic the effect of anomalous resistivity resulting from a current driven instability (Sato & Hayashi, 1979), used a local resistivity enhancement that depended linearly on the current density. They found that this setup lead to fast magnetic reconnection. These results were corroborated by Ugai (1984), who employed different current-dependent resistivity models. Yan et al. (1993) studied reconnection with a combination of uniform and localized resistivity and found that the diffusion region length and width scale with the localization of the resistivity. Additionally, they found, consistent with analytical predictions, that for uniform resistivity the diffusion region tends to lengthen and evolves slowly. Kulsrud (2001) suggested that a Petschek-type reconnection rate can be induced if there is a gradient in the resistivity. This hypothesis was confirmed by a recent study by Lin et al. (2021). It shows that fast reconnection can be achieved using a 1D hyperbolic tangent resistivity profile varying along the outflow direction, obtaining a maximum rate value of ≈0.2.

In a collisionless plasma, resistivity is generally thought to be provided by either wave-particle interactions (anomalous resistivity) or meandering electron trajectories associated with non-gyrotropic electron distributions in the vicinity of the X line (e.g., Hesse et al., 1999). Recent spacecraft observations have demonstrated the prevalence of such electron distributions in reconnecting environments (e.g., Torbert et al., 2018), supporting the meandering electron reconnection model. However, the role of waves is still being actively investigated (e.g., Chen et al., 2020; Graham et al., 2017).

The purpose of the present study is to investigate numerically whether there are upper limits to the reconnection rate in a current sheet, and whether such limits depend on certain properties of the diffusion region. We investigate this question by ad-hoc variations of amplitude and shape of a resistive spot in MHD simulations. We acknowledge that, in collisionless plasmas, microphysical processes determine properties of the diffusion region. Consequently, not all shapes or amplitudes of our resistive region may be reproduced by processes in nature. This implies that the reconnection rates should be interpreted as upper limits of what might be found in real plasmas.

We use a 2D resistive MHD model to study how effective the reconnection rate can be by varying magnitudes and shapes of a localized resistivity centered at the x-line. Furthermore, we analyze the physics inside the diffusion region using the induction equation, which allows us to identify the contribution of advection and diffusion to the current profile. The highest rate in our series of simulations is found for very high magnitudes of the resistivity, combined with a specific choice of the aspect ratio. This maximum value is close to 0.25 in normalized units, which is similar to the 0.2 value predicted by Liu et al. (2017).

The paper is organized as follows: In Section 2, we describe the simulation setup employed in this study. In Section 3 we investigate the impact of the magnitude of the resistivity on the reconnection rate and the diffusion region. In Section 4 we study the impact of the shape of the resistive region on the reconnection rate and the diffusion region. Section 5 is a summary of our results with some discussion.

2. Simulation Setup

The study is performed using 2D MHD simulations, which solve the time-dependent resistive MHD equations using an explicit finite-difference method. More on this has previously been described in detail by Birn and Hones (1981). The governing equations are:

$$\partial_t \rho = -\nabla \cdot (\rho \mathbf{v}) \tag{1}$$

$$\partial_t (\rho \mathbf{v}) = \nabla \cdot (\rho \mathbf{v}\mathbf{v} - \mathbf{P} + \mathbf{M}) \tag{2}$$

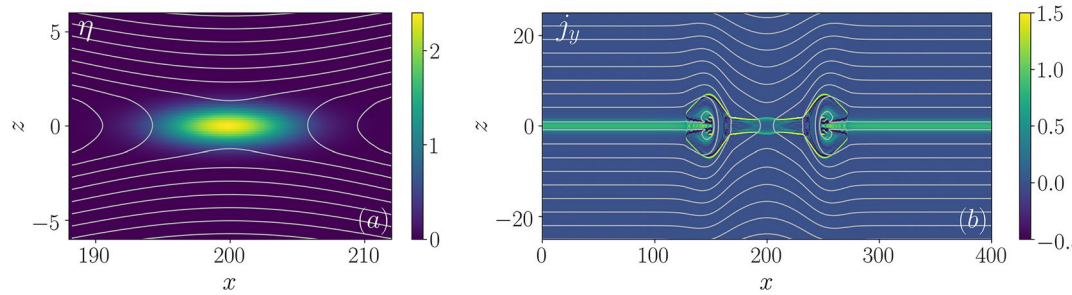

Figure 1. Simulation overview at timestep $t = 50$ for $\eta_1 = 2.4$, $L_x = 5$ and $L_z = 1$. (a) Resistivity profile as a function of x and z. (b) Current density profile as a function of x and z. The gray lines indicate constant values of the vector potential, (A).

$$\partial_t \mathbf{B} = \nabla \times (\mathbf{v} \times \mathbf{B}) + \eta \nabla^2 \mathbf{B} - \nabla \eta \times \mathbf{j} \tag{3}$$

$$\partial_t u = -\nabla \cdot (u\mathbf{v}) + \frac{\gamma - 1}{\gamma} u^{1-\gamma} \eta j^2 \tag{4}$$

where η is the resistivity, $\gamma = 5/3$ is the adiabatic index, u is defined as $u = p^{1/\gamma}$ (Birn, 1980) and $\mathbf{M}$ is the Maxwell Stress Tensor, defined by $M_{ij} \equiv \frac{1}{\mu_0} B_i B_j - \frac{1}{2\mu_0} B^2 \delta_{ij}$. The permeability μ_0 is set to one in code unit. Equations 1 and 2 are the mass and momentum conservation equations, respectively. Equation 3 is the induction equation, which describes the evolution of the magnetic field. We use the resistive Ohm's law to determine the electric field: $\mathbf{E} = -\mathbf{v} \times \mathbf{B} + \eta \mathbf{j}$. Equation 4 is the conservation law for thermal energy.

The simulation takes place in a simulation domain large enough to prevent any boundary effects intervening with the reconnection process. Our simulation domain is 400×200, with x going from 0 to 400 and z from -100 to 100, distributed over $3{,}200 \times 1{,}600$ cells. The boundary conditions consist of solid and ideally conducting walls at the top and bottom of the box, while the left and right walls are periodic. The code runs on the Alfvén timescale, where $t = L/v_A$ and L is the characteristic length scale, corresponding to the distance an Alfvén wave can travel in a time unit. The computational time step is $dt = 0.0125$.

The initial condition in our simulation consists of a two-dimensional Harris-type equilibrium (Harris, 1962), in which the magnetic field is $\mathbf{B}(z) = \tanh(z/L)\hat{\mathbf{x}}$, where L is unity. The plasma density is $\rho = \mathrm{sech}^2(z/L) + \rho_0$, where ρ_0 is the plasma density at the inflow, and the plasma pressure is given by $p = \rho T$, where T is the sum of the electron and ion temperature and fulfill $T = T_i + T_e = 0.5$. This leads to $p = 1/2\ \mathrm{sech}^2(z/L) + p_0$, with $p_0 = T\rho_0$. The coordinate system is as follows: x is the reconnection outflow direction, y is the current direction and z is the inflow direction.

The total resistivity, η consists of a background resistivity (η_0) plus an exponential function in the center of the box given by

$$\eta = \eta_0 + \eta_1 e^{-\left[\left(\frac{x - x_{\max}/2}{L_x}\right)^2 + \left(\frac{z}{L_z}\right)^2\right]}. \tag{5}$$

Here, η_1 determines the peak magnitude of the resistivity, while L_x and L_z determine the shape of the resistive region. Figure 1a shows the resistivity profile for a background resistivity of $\eta_0 = 0.0015$, a peak resistivity of $\eta_1 = 2.4$ and an aspect ratio of $L_x/L_z = 5$ as a function of x and z.

Figure 1b shows the out-of-plane current density profile at timestep $t = 50$. The gray lines indicate constant values of the vector potential, $\mathbf{A}$, defined as $\mathbf{B} = \nabla \times \mathbf{A}$, or magnetic field lines. At this time, the inflowing magnetic field lines are considerably deformed compared to their initial state as a consequence of their expansion toward the reconnection region. This effect is amplified by the outflow structures that can be observed around $x = 150$ and 250 in the current density. Similar outflow structures were also found by Zenitani et al. (2009), and we refer to that paper for a description on the associated outflow dynamics. In this paper we focus on the reconnection rate and the behavior and dynamics surrounding the diffusion region.

With the described simulation setup, we will now investigate how the reconnection rate scales with different values of the magnitude and the shape of the resistive region. A total of 32 runs have been carried out. Table 1

Table 1
Simulation Parameters for 6 Selected Runs for Each Part of the Study

Run	η_1	L_x	L_z	Peak rate	Run	η_1	L_x	L_z	Peak rate
M1	3×10^{-3}	5	1	0.019	S1	2.4	0.5	1	0.224
M2	1.5×10^{-2}	5	1	0.053	S2	2.4	2	1	0.254
M3	7.5×10^{-2}	5	1	0.103	S3	2.4	5	1	0.203
M4	0.3	5	1	0.158	S4	2.4	8	1	0.157
M5	1.5	5	1	0.198	S5	2.4	15	1	0.075
M6	2.4	5	1	0.203	S6	2.4	40	1	0.020

Note. M stands for magnitude, while S stands for shape. η_1, L_x and L_z correspond to the parameters written in Equation 5. η_1 corresponds to the value of the resistivity at the x-line. L_x and L_z describe the shape of the resistive region. The last column in each table indicates the peak reconnection rate for each of the runs.

specifies the value of the magnitude of the resistivity (η_1), L_x, L_z and the maximum reconnection rate for 6 selected runs for each part of the study.

3. Impact of the Magnitude of the Resistivity

In this section, we investigate how the system responds to different magnitudes of localized resistivity. Figure 2a shows the time evolution of the reconnection rate for the 6 M runs specified in Table 1. Reconnection rates in these simulations are calculated using the in-to-plane electric field at the x-line, $E_{y,xline} = \eta_{xline} j_{y,xline}$. They are normalized as $R \equiv E_{y,xline}/(B_0 v_{A0})$ where B_0 is the inflow magnetic field and $v_{A0} = B_0/\sqrt{\rho_0}$, calculated with the same inflow magnetic field and the Harris sheet density ($\rho_0 = 1$). Note that our inflow density has a value of $\rho_{in} = 0.2\rho_0$, and the value of the reconnection rate would change if normalized to this quantity. As follows, $R_{in} = \sqrt{\rho_{in}/\rho_0}R \sim \sqrt{0.2}R$, where R_{in} is the reconnection rate normalized to the inflow Alfvén speed.

In runs M1 and M2, the reconnection process is very slow, resulting in a slow evolution of the system. As a consequence, the peak reconnection rate is reached at much later time steps than for the other 4 cases. Runs M3, M4, and M5 have a significantly faster evolution, reaching their peak at earlier time steps. Run M6, despite being the fastest, does not vary significantly from M5, indicating that the rate saturates or is limited. The decrease in the reconnection rate after the peak is a result of finite amount of flux in our simulations domain. The initial growth of the reconnection rate for large enough values of the gradient of the resistivity (see runs M3 to M6 in Figure 2a) is given by the term $\nabla\eta \times \mathbf{j}$. It is clear that this initial evolution scales as R_m^{-1}, where R_m is the magnetic Reynolds number.

Figure 2b shows the peak reconnection rate as a function of η_1 for the 16 runs carried out. The colored stars correspond to the labeled runs in panel a. For weak resistivities ($\eta_1 \lesssim 0.5$), the reconnection rate is slow but increases rapidly with increasing values of η. For strong resistivities ($\eta_1 \gtrsim 1$), the rapid increase ceases, and the rate saturates at approximately 0.2. This behavior illustrates that the effect of increased resistivity can significantly influence the reconnection rate, but only to a certain level.

The solid blue line in Figure 2b represents the function $f(\eta_1) = \frac{a\eta_1}{b+\eta_1} + c$, where $a = 0.2$, $b = 0.1$ and $c = 0.01$. The function describes the behavior of the reconnection rate with great accuracy. The value of a relates to the maximum reconnection rate and has dimensions corresponding to the electric field. The value of b determines how quickly the function converges, and has dimensions corresponding to η. It is possible that the constant c is related to the uniform background resistivity η_0, signifying a constant energy conversion throughout the simulation domain.

Thus, even if we enable the diffusion region to support extreme diffusion, the reconnection rate appears to be controlled and limited by properties on larger scales. This result is in agreement with Lin et al. (2021), who found that the reconnection rate is bounded by physics outside of the diffusion region, and with Liu et al. (2017) who suggested this limitation to be related to the force-balance in the upstream region.

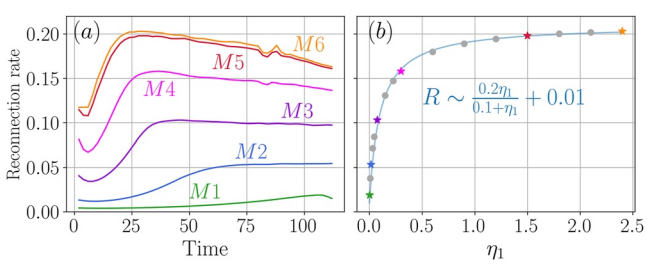

Figure 2. (a) Time evolution of the reconnection rate for the six runs specified in Table 1. The colored labels indicate which run we are referring to. (b) Peak reconnection rate as a function of η_1 for all 16 runs. The colored $*$'s correspond to the runs in panel (a). Note that the reconnection rate is bounded by a value $\simeq$0.2. The solid blue line represents a fit to the data, with the function written in the panel.

In Figure 3, we investigate the behavior of the reconnection rate for the runs M3 and M6 at the time of peak reconnection rate. These runs are identical except for different values of η_1. Panels 3a and 3days show the current density profile, j_y, in blue and the resistivity profile, η, in orange as a function of z in a cut along x through the x-line. The current density profiles are distinctly different between the runs: For Run M3 ($\eta_1 = 0.075$), the current density has a peak at the x-line, while M6 ($\eta_1 = 2.4$) has a bifurcated current sheet with a significantly decreased j_y at the $z = 0$.

The product of the resistivity and the current density yields the reconnection electric field, and it is clear that as η increases, the current density distribution is altered to limit the rate at the center. As the width of the current sheet increases, the regions of enhanced current density move toward the edge of

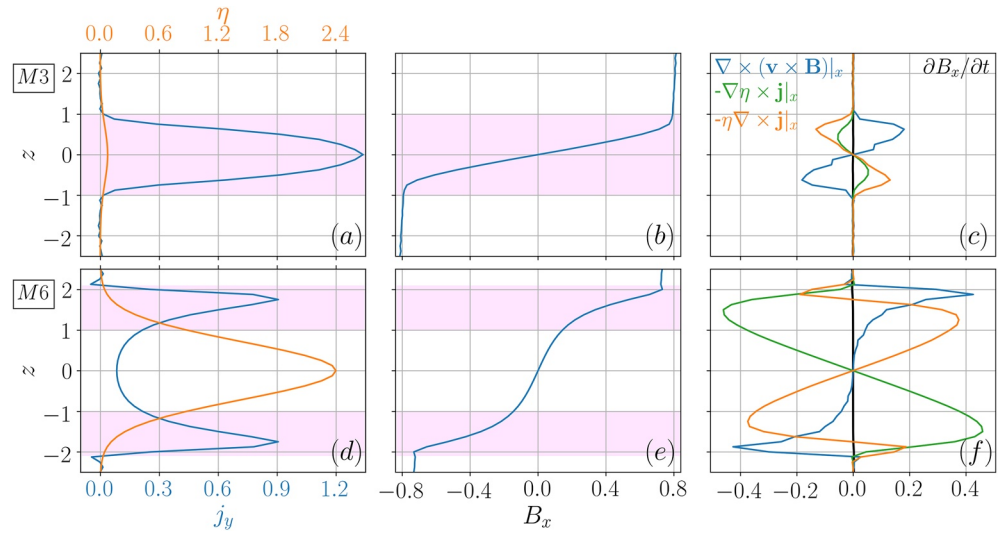

Figure 3. Comparison of diffusion region for the runs M3 (a)–(c) and M6 (d)–(f) at the time of their peak reconnection rate. (a) and (d) Current density profile in blue and resistivity profile in orange as a function of z. Note that the current density drops significantly at the x-line for M6.(b) and (e) Inflow magnetic field profile. The pink shaded areas indicate where the gradient in B_x is largest, corresponding to the peaks in the current density, j_y. (c) and (f) Contribution of the different terms of the induction equation. In black: time derivative of B_x. In blue: advection term. In green and orange: resistive terms.

the diffusion region, as indicated by the highlighted areas in panel 3d. These peaks in the current density are determined by the curl of the magnetic field, described by Ampère's Law. Panels 3b and 3e show the profile of B_x, with the corresponding areas with the largest gradient highlighted. For the run M6, the gradient of the reconnecting magnetic field (B_x) has been forced toward the edge of the diffusion region, effectively reducing the magnitude around the x-line.

A reconfiguration of the current sheet width involves a change of the magnetic field distribution. The evolution of the magnetic field is given by Faraday's law, $\frac{\partial \mathbf{B}}{\partial t} = -\nabla \times \mathbf{E}$, where $\mathbf{E}$ in our case is given by the resistive Ohm's law: $\mathbf{E} = -\mathbf{v} \times \mathbf{B} + \eta \mathbf{J}$. The induction equation can then be expressed as:

$$\partial_t B_x = \nabla \times (\mathbf{v} \times \mathbf{B}) \mid_x - \eta \nabla \times \mathbf{j} \mid_x - \nabla \eta \times \mathbf{j} \mid_x . \tag{6}$$

We evaluate this equation at the inflow region.

The first term in the right-hand side of this equation corresponds to the advection of magnetic flux, whereas the second term corresponds to the diffusion of magnetic flux due to gradients in the current density. The final term enables us to study the role and effect of resistivity gradients on the diffusion. To investigate which terms are responsible for the creation of the bifurcated current profile we show the contribution of each of these terms for the runs M3 and M6 in a cut along the x-direction through the x-line in Figures 3c and 3f.

In both runs, the temporal variation of B_x (black line) is negligible. This is expected as the system has already established the magnetic field and associated current structure, neither of which move or change significantly in magnitude. The advective term (blue line) has a positive value for $z > 0$, which means that it is trying to increase B_x by transporting new field lines into the region. The green and orange lines show the contribution from diffusion to the profile of B_x. The diffusion in B_x enables the formation of new magnetic connections and will result in an increased B_z in the outflow region. Since $\partial B_x/\partial t$ is almost zero, there must exist a balance between the advective and diffusive terms, which means that the flux is being diffused at the same rate at which it is being transported into the diffusion region.

Run M3 has a small gradient in η, which results in a small contribution by the $-\nabla\eta \times \mathbf{j}$ term (green line). Consequently, more flux is being transported into the diffusion region by the advective term (blue line) than being diffused away by the gradient of the resistivity. However, adding the contribution from the gradient of the current density (orange line) establish the balance. This enables the system to maintain a current sheet with a

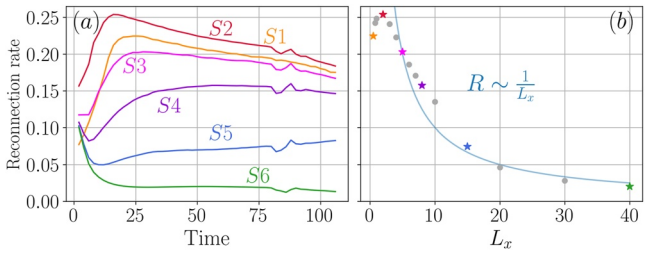

Figure 4. (a) Time evolution of the reconnection rate for the six runs specified in Table 1. The colored labels indicate which run are we referring to. (b) Peak reconnection rate as a function of L_x for all 17 runs. Note that the maximum reconnection rate is achieved for $L_x = 2$.

characteristic current density profile (as seen in panel a). Thus, the current sheet profile is maintained by the balance between advection of fresh flux and diffusion by both the gradient of η and the current density.

Run M6 has an extremely large gradient in η, which results in a large contribution by the term $-\nabla\eta \times \mathbf{j}$. This is evident by looking at the green line in Figure 3f. This large gradient in the resistivity forces the flux to be diffused away in a very short spatial scale, which results in a rapid decrease of the advective term (blue line). For $z > 0$, we observe the negative contribution of the green line, together with the rapid decrease in the positive advective term around $z \approx 1.8$. The term related to the curl of the current density (orange line) is negative for $z \gtrsim 1.8$, but has a positive contribution for $0 < z \lesssim 1.8$. This term tries to diffuse the bifurcated peak in both directions (toward $z = 0$ and to $z > 1.8$). Compared to panel c, the advective contribution to the magnetic field gradient close to the x-line in panel f is dominated by this diffusion of the current peak. Thus, the distribution of the orange diffusive term allows a finite j_y at the x-line, which is necessary for reconnection to operate. This is how the system is able to maintain a finite reconnection rate.

The expression in the functional fit is describes the gradient length scale of the term accounting for the gradient in the resistivity. Although by design, this gradient length scale is the same for all the different runs since the resistivity has a fixed shape. However, as the magnetic field gradients are forced outwards from the current sheet, resulting in a bifurcated current sheet, the local value of this gradient length scale changes. We suggest that the functional fit captures this effect.

4. Impact of the Shape of the Resistive Spot

In the previous section, we saw that the reconnection rate increases when increasing the magnitude of the resistivity, but only up to a value of around 0.2. The reconnection rate is limited by the bifurcation of the current sheet when the gradients of the magnetic field are pushed out of the diffusion region, which results in a reduced current density around the x-line. Now, we take the highest value of the magnitude of the resistivity from the previous section ($\eta_1 = 2.4$), to study how the reconnection rate varies when changing the shape of the resistive region. This is achieved by varying the x-extent of the resistivity while keeping a constant z-extent.

Figure 4a shows the time evolution of the reconnection rate for the 6 different runs specified in Table 1 in the same format as Figure 2. Note that run S3 is equivalent to run M6. The small perturbation that appears at around $t = 85$ is due to a small perturbation in E_y created at the center of the current sheet at $t = 0$. This perturbation travels to the edge of the box, reflects and reaches the current sheet again at around $t = 85$, slightly modifying the reconnection rate. This is a boundary effect that has no influence on the results of our study.

In Figure 4b, we have plotted the peak reconnection rate as a function of L_x for all 17 runs carried out. The peak reconnection rate has a value of around 0.25. This maximum value is reached for run S2, which has an aspect ratio of $L_x/L_z = 2$. The slowest reconnection rates are reached for the largest values of L_x, as expected as the diffusion region becomes very elongated. This resembles the original Sweet-Parker description (Parker, 1957; Sweet, 1958), where the length of the diffusion region is comparable to the system scale. The rate becomes very small since there is no significant tension on the reconnected field lines to transport the flux away.

For large aspect ratios, we would expect the reconnection rate to scale as predicted by the Sweet-Parker scaling, $R \sim L_z/L_x = 1/L_x$. This function has been plotted as a blue line in Figure 4b. As expected, the function fits with the data only for very large aspect ratios ($L_x/L_z > 15$). However, it does not reproduce the behavior of the reconnection rate for smaller aspect ratios.

For $L_x \lesssim 2$, the peak reconnection rate decreases with decreasing L_x. The reconnection rate is proportional to the current density at the x-line, since $E_{y,xline} = \eta_{xline} j_{y,xline}$ and η_{xline} is the same for all the runs in this part. Figure 5a shows the out of plane current density in a cut along $z = 0$ for S1, S2, and S3. Accordingly, j_y at the x-line is largest for S2. We also note that the distribution of the current density is significantly different for the three choices of L_x. This directly reflects the influence of the resistive shape on the gradients of the magnetic field. The highest current density is seen adjacent to the x-line for S1, while S2's profile is slightly wider and has a lower peak

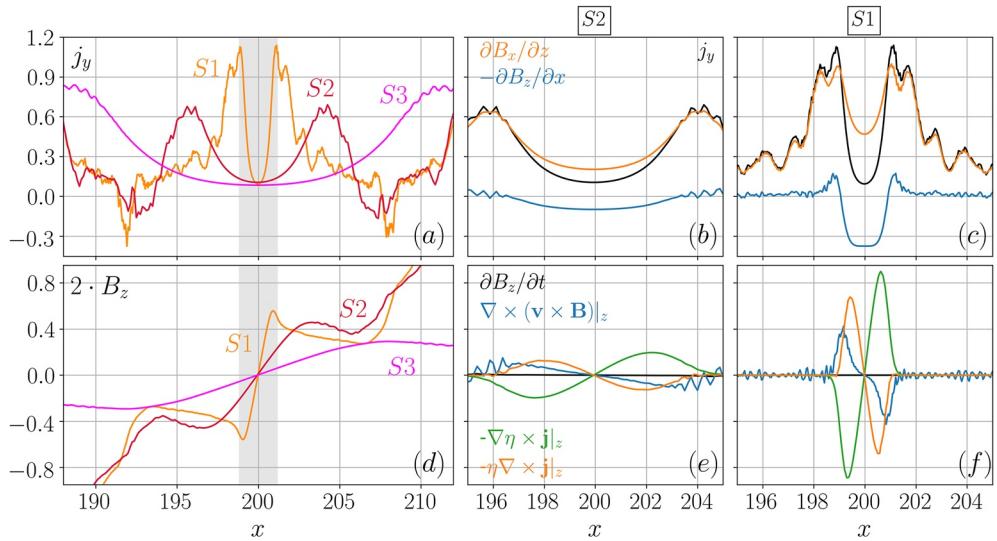

Figure 5. Comparison of diffusion region for cases where $L_x \leq 2$ at the time of their peak reconnection rate in a cut along $z = 0$. (a) j_y as a function of x for S1, S2, and S3. Note that S2 has the highest current density at the x-line, which corresponds to the fastest reconnection rate. (b) and (c) Different terms of the equation $\mathbf{j} = \nabla \times \mathbf{B}$ contributing to the out of plane current density for S1 and S2. (d) Outflow magnetic field as a function of z for S1, S2 and S3. Note the enhancement near the x-line for the run S1. The quantity has been multiplied by a factor two for esthetic reasons. (e) and (f) Contribution of the induction terms for S1 and S2.

magnitude. For S3, the current density is distributed over a larger area. Hence, the distance between the peaks adjusts to the width of the resistive region for each of the runs.

In Figure 5d, we show the outflow magnetic field, B_z (multiplied by a factor of 2) at $z = 0$ as a function of x. Note that the strength of B_z of the reconnected magnetic field decreases for larger L_x: $\nabla \cdot \mathbf{B} = 0 \Rightarrow B_z \sim \frac{B_x L_z}{L_x}$. In this panel, we can see how the magnetic field gradients coincide with the current density profile. The shaded area highlights the large gradient in B_z around the x-line for the case S1. Figures 5b and 5c show the out of plane current density as a function of x for the runs S2 and S1, respectively. To determine how each magnetic field component contributes to the current density, we show both terms of Ampère's law, $j_y = \nabla \times \mathbf{B}|_y = \partial B_x/\partial z - \partial B_z/\partial x$. For the run S1 there is a large contribution of $\partial B_z/\partial x$ at the x-line, which subtracted from $\partial B_x/\partial z$ results in a smaller current density than S2 (see panel b) and, consequently, a lower reconnection rate.

Hence, for $L_x \lesssim 2$, the large enhancement of B_z close to the x-line results in a lower reconnection rate. This enhancement must be due to the large resistivity gradient in the x direction appearing when η has an extremely short x-extent. Figures 5e and 5f show the contribution of the advective and resistive terms to the variation of B_z, in a similar way as in Figures 3c and 3f. Panel 5f shows the large contribution of the $\nabla\eta \times \mathbf{j}|_z$ term (green) to the B_z profile. For $x > 200$, we note that this term is the only positive contribution to B_z, while the other two terms have a negative contribution which balances the former when a quasi-steady state is reached. Contrary to S1, for the run S2 η has a larger extent, which results in a contribution of the green term more distributed over space and a smaller B_z (see panel e). This confirms that the large gradient in B_z appears due to the short extent of the strong resistive region in the x-direction.

The scaling function in Figure 5b does not capture the effects of the gradient of B_z for small aspect ratios. This effect accounts for at least parts of the discrepancy between the functional fit and the data. For large aspect ratios, $\partial B_z/\partial x$ is negligible, and the change in the current density is fully determined by $\partial B_x/\partial z$.

5. Summary and Discussion

We have shown that increasing the magnitude of the resistivity in our system indeed results in an increased reconnection rate, but only to a value of about 0.25. For high magnitudes of the resistivity, the rate is limited by the bifurcation of the current sheet. To maintain the balance between advection and diffusion, the gradient of the

magnetic field is pushed toward the boundary of the diffusion region, resulting in a smaller current density at the center, and a limited reconnection rate.

The bifurcation of the current sheet occurs when the flux is being diffused at a faster rate than it is being transported into the diffusion region. In our case, we observe a current sheet bifurcation for the runs M4, M5 and M6, but not for M1, M2 and M3. Thus, the transition occurs between M3 and M4. Equation 6 is used to analyze the rates of advection and diffusion in both runs. Written in terms of characteristic quantities, Equation 6 becomes

$$\frac{B}{\tau} \sim \frac{vB}{L_B} - \frac{\eta B}{L_D L_B}, \tag{7}$$

where τ represents the time scale, L_D represents the effective diffusion length in the z direction and L_B represents the length scale of the magnetic field. Multiplying the whole equation by L_B we get the flux per unit time processed:

$$\frac{BL_B}{\tau} \sim vB - \frac{\eta B}{L_D}. \tag{8}$$

The first term on the right-hand side represents the flux transported by the advection term, while the second term represents the flux processed by the diffusion term. To estimate the contribution we assume that the incoming magnetic field has a value of 1 (equal to the initial inflow magnetic field strength). L_D is determined when we define the resistive spot and does not change between these runs. It corresponds to $L_z = 1$. For run M3, the inflow velocity is ≈0.1. Then, the advection term transports flux into the diffusion region at a rate of ≈0.1, while the diffusion rate is approximately 0.075 ($\partial B_x/\partial z = J_y \approx 1$) for $\eta = 0.075$. Accordingly, since $vB > \frac{\eta B}{L_D}$, the diffusion will be distributed throughout the entire diffusion region. In M4, the inflow velocity is ≈0.2. Consequently, the diffusion region can diffuse the magnetic field at a higher rate (≈0.3 for $\eta_1 = 0.3$) than the advective term can transport fresh flux into the region (≈0.2). As a result, the flux is diffused over a shorter length scale, resulting in a bifurcated current sheet.

Bifurcated current sheets are frequently observed in space by in situ spacecraft (Hoshino et al., 1996; Runov et al., 2006). In this study, we have shown that the current sheet bifurcation occurs as a result of an imbalance between the diffusion rate and the transport rate. In nature, the diffusion is set up self-consistently (Hesse et al., 2018). Thus, we have to relate our enhanced diffusion rate to a physical process that could have the same properties. Many theoretical and simulation efforts have been made to find the origin of the current sheet bifurcation (Sitnov et al., 2004; Zelenyi et al., 2003). A recent study by Jiang and Lu (2021) found that the bifurcated profile of the current density is caused by an electron pressure anisotropy formed at the center of the current sheet, which decreases the current density at the center. This pressure anisotropy may be the trigger for our diffusion enhancement in MHD. Other studies have shown that the bifurcated current is largely carried by diamagnetic drifts associated with non-gyrotropic electron distributions (Norgren et al., 2018).

When varying the shape of the diffusion region, we demonstrated that there is a maximum reconnection rate for an aspect ratio of $L_x/L_z = 2$. We showed that for very small aspect ratios, the resistivity gradient in the x direction is so large that it influences the J_y at the X-point, and consequently reduces the reconnection rate. One can relate the extent of the resistive region to the aspect ratio of the diffusion region by L_x and L_z. Liu et al. (2017) showed that the reconnection rate has a maximal value for an intermediate opening angle of the separatrix, which is related to the shape of the diffusion region. The $\mathbf{J} \times \mathbf{B}$ force driving the outflow becomes smaller as the opening angle increases. The tension force is canceled by the magnetic pressure force when the separatrices form an angle of 90°, stopping reconnection. For small opening angles, the $\mathbf{J} \times \mathbf{B}$ also becomes smaller as the opening angle decreases, since the z component of the reconnected magnetic field decreases. Thus, an optimal opening angle must exist, which, in our case, is achieved in the run $S2$, for $L_x = 2$ and $L_z = 1$.

Figure 6 shows magnetic field lines for 4 different runs: S1, S2, S3, and S4. These lines have been plotted using constant values of the magnetic vector potential, $\mathbf{A}$, defined by $\mathbf{B} = \nabla \times \mathbf{A}$. For each of the runs there is an inflow magnetic field line and a reconnecting magnetic field line. The highest reconnection is obtained for $L_x = 2$, which has a opening angle of ∼15° (S2 in Figure 6). The opening angle is comparable to the analytically predicted value of ∼17°, suggested by Liu et al. (2017). Figure 6) shows a clear trend in the opening angle versus the reconnection rate. As L_x decreases from 8 (S4) to 2 (S2), the opening angle increases, which consistently means that the

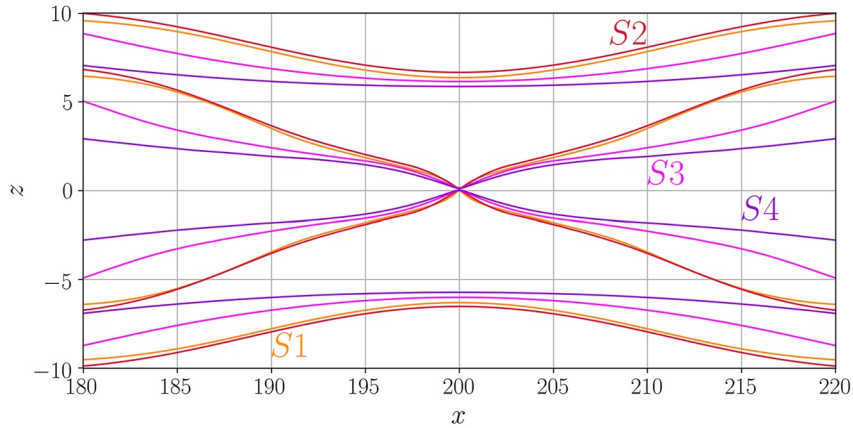

Figure 6. Magnetic field lines for S1, S2, S3, and S4. Each run has one field line in the inflow, one field line in the outflow, and one reconnecting field line. Colors indicate which run the line is referring to.

outflow driving force increases, accordingly with the reconnection rate. However, for values between $L_x = 2$ (S2) to $L_x = 0.5$ (S1), we observe a macroscopic decrease of the opening angle, contrary to what we would expect at microscopic scales. This is still consistent with the reduction of j_y. The current density, the outflow force and velocity, the reconnection rate, and the opening angle are coupled and self-consistently regulated between microscopic and macroscopic scales. The maximum reconnection rate is achieved when the different properties of the reconnection site conspire to allow and support an optimum opening angle. In the inflow region, different levels of field line deformation can be observed for the different runs. This deformation is related to the opening angle of the separatrix.

In summary, the present study shows that when inserting very strong resistive spots with varying shapes, there appears to be a maximum rate of reconnection the system can support. In addition, a sub-optimal choice of the magnitude and shape of the resistive spot leads to lower overall reconnection rates. This implies that the reconnection rate depends significantly on the properties of the diffusion region, even if the size of that region is much smaller than the system. However, there are also very strong indications that the rate of reconnection is limited due to larger-scale system properties.

Data Availability Statement

Data for this paper is available at Pérez-Coll Jiménez (2021).

Acknowledgments
This study was supported by the Research Council of Norway under contract 300865. The simulations were performed on resources provided by UNINETT Sigma2 – the National Infrastructure for High Performance Computing and Data Storage in Norway under project NN9496k.

References

Angelopoulos, V., McFadden, J. P., Larson, D., Carlson, C. W., Mende, S. B., Frey, H., et al. (2008). Tail reconnection triggering substorm onset. *Science*, *321*(5891), 931–935. https://doi.org/10.1126/science.1160495

Birn, J. (1980). Computer studies of the dynamic evolution of the geomagnetic tail. *Journal of Geophysical Research*, *85*(A3), 1214–1222. https://doi.org/10.1029/ja085ia03p01214

Birn, J., & Hones, Jr, E. W. (1981). Three-dimensional computer modeling of dynamic reconnection in the geomagnetic tail. *Journal of Geophysical Research*, *86*(A8), 6802–6808. https://doi.org/10.1029/ja086ia08p06802

Cassak, P. A., Liu, Y.-H., & Shay, M. A. (2017). A review of the 0.1 reconnection rate problem. *Journal of Plasma Physics*, *83*(5), 715830501. https://doi.org/10.1017/S0022377817000666

Chen, L. J., Wang, S., Le Contel, O., Rager, A., Hesse, M., Drake, J., et al. (2020). Lower-hybrid drift waves driving electron nongyrotropic heating and vortical flows in a magnetic reconnection layer. *Physical Review Letters*, *125*(2), 025103. https://doi.org/10.1103/PhysRevLett.125.025103

Drake, J. F., Kleva, R. G., & Mandt, M. E. (1994). Structure of thin current layers: Implications for magnetic reconnection. *Physical Review Letters*, *73*, 1251–1254. https://doi.org/10.1103/physrevlett.73.1251

Genestreti, K. J., Nakamura, T. K. M., Nakamura, R., Denton, R. E., Torbert, R. B., Burch, J. L., et al. (2018). How accurately can we measure the reconnection rate em for the mms diffusion region event of 11 July 2017? *Journal of Geophysical Research: Space Physics*, *123*(11), 9130–9149. https://doi.org/10.1029/2018ja025711

Graham, D., Khotyaintsev, Y., Vaivads, A., Norgren, C., André, M., Webster, J., et al. (2017). Instability of agyrotropic electron beams near the electron diffusion region. *Physical Review Letters*, *119*. https://doi.org/10.1103/PhysRevLett.119.025101

Harris, E. G. (1962). On a plasma sheath separating regions of oppositely directed magnetic field. *Il Nuovo Cimento - B*, *23*(1), 115–121. https://doi.org/10.1007/BF02733547

Hesse, M., Liu, Y. H., Chen, L. J., Bessho, N., Wang, S., Burch, J. L., et al. (2018). The physical foundation of the reconnection electric field. *Physics of Plasmas*, *25*(3), 032901. https://doi.org/10.1063/1.5021461

Hesse, M., Neukirch, T., Schindler, K., Kuznetsova, M., & Zenitani, S. (1999). The diffusion region in collisionless magnetic reconnection. *Physics of Plasmas*, *6*(5), 1781–1795. https://doi.org/10.1063/1.873436

Hoshino, M., Nishida, A., Mukai, T., Saito, Y., Yamamoto, T., & Kokubun, S. (1996). Structure of plasma sheet in magnetotail: Double-peaked electric current sheet. *Journal of Geophysical Research*, *101*(A11), 24775–24786. https://doi.org/10.1029/96ja02313

Jiang, L., & Lu, S. (2021). Externally driven bifurcation of current sheet: A particle-in-cell simulation. *AIP Advances*, *11*(1), 015001. https://doi.org/10.1063/5.0037770

Kulsrud, R. (2001). Magnetic reconnection: Sweet-parker versus petschek. *Earth Planets and Space*, *53*, 417–422. https://doi.org/10.1186/BF03353251

Li, X., & Liu, Y.-H. (2021). The effect of thermal pressure on collisionless magnetic reconnection rate. *The Astrophysical Journal*, *912*(2), 152. https://doi.org/10.3847/1538-4357/abf48c

Lin, S.-C., Liu, Y.-H., & Li, X. (2021). Fast magnetic reconnection induced by resistivity gradients in 2d magnetohydrodynamics. *Physics of Plasmas*, *28*(7), 072109. https://doi.org/10.1063/5.0052317

Liu, Y.-H., Hesse, M., Guo, F., Daughton, W., Li, H., Cassak, P. A., & Shay, M. A. (2017). Why does steady-state magnetic reconnection have a maximum local rate of order 0.1? *Physical Review Letters*, *118*(8), 1–6. https://doi.org/10.1103/PhysRevLett.118.085101

Liu, Y.-H., Li, T. C., Hesse, M., Sun, W. J., Liu, J., Burch, J., et al. (2019). Three-dimensional magnetic reconnection with a spatially confined x-line extent: Implications for dipolarizing flux bundles and the dawn-dusk asymmetry. *Journal of Geophysical Research: Space Physics*, *124*(4), 2819–2830. https://doi.org/10.1029/2019ja026539

Masuda, S., Kosugi, T., Hara, H., Tsuneta, S., & Ogawara, Y. (1994). A loop-top hard X-ray source in a compact solar flare as evidence for magnetic reconnection. *Nature*, *371*(6497), 495–497. https://doi.org/10.1038/371495a0

Norgren, C., Graham, D. B., Khotyaintsev, Y. V., André, M., Vaivads, A., Hesse, M., & Russell, C. T. (2018). Electron reconnection in the magnetopause current layer. *Journal of Geophysical Research: Space Physics*, *123*(11), 9222–9238.

Parker, E. N. (1957). Sweet's mechanism for merging magnetic fields in conducting fluids. *Journal of Geophysical Research*, *62*(4), 509–520. https://doi.org/10.1029/JZ062i004p00509

Parker, E. N. (1963). The solar-flare Phenomenon and the theory of reconnection and annihiliation of magnetic fields. *The Astrophysical Journal*, *8*, 177. https://doi.org/10.1086/190087

Parker, E. N. (1973). The reconnection rate of magnetic fields. *The Astrophysical Journal*, *180*, 247–252. https://doi.org/10.1086/151959

Pérez-Coll Jiménez, J. (2021). *Replication data for: The role of resistivity on the efficiency of magnetic reconnection in mhd*. https://doi.org/10.18710/HK6CV6

Petschek, H. E. (1964). *Magnetic Field Annihilation* (Vol. 50, p. 425). Nasa special publication.

Runov, A., Sergeev, V. A., Nakamura, R., Baumjohann, W., Apatenkov, S., Asano, Y., et al. (2006). Local structure of the magnetotail current sheet: 2001 cluster observations. *Annales Geophysicae*, *24*(1), 247–262. https://doi.org/10.5194/angeo-24-247-2006

Sato, T., & Hayashi, T. (1979). Externally driven magnetic reconnection and a powerful magnetic energy converter. *The Physics of Fluids*, *22*(6), 1189–1202. https://doi.org/10.1063/1.862721

Shibata, K., & Magara, T. (2011). Solar flares: Magnetohydrodynamic processes. *Living Reviews in Solar Physics*, *8*(1), 6. https://doi.org/10.12942/lrsp-2011-6

Sironi, L., Petropoulou, M., & Giannios, D. (2015). Relativistic jets shine through shocks or magnetic reconnection? *Monthly Notices of the Royal Astronomical Society*, *450*(1), 183–191. https://doi.org/10.1093/mnras/stv641s

Sitnov, M. I., Swisdak, M., Drake, J. F., Guzdar, P. N., & Rogers, B. N. (2004). A model of the bifurcated current sheet: 2. Flapping motions. *Geophysical Research Letters*, *31*(9). L09805. https://doi.org/10.1029/2004gl019473

Sweet, P. A. (1958). The neutral point theory of solar flares. In B. Lehnert (Ed.) *Electromagnetic phenomena in cosmical physics*, (Vol. 6, pp. 123–134). https://doi.org/10.1017/s0074180900237704

Tenfjord, P., Hesse, M., Norgren, C., Spinnangr, S. F., & Kolstø, H. (2019). The impact of oxygen on the reconnection rate. *Geophysical Research Letters*, *46*(12), 6195–6203. https://doi.org/10.1029/2019GL082175

Toledo-Redondo, S., André, M., Aunai, N., Chappell, C. R., Dargent, J., Fuselier, S. A., & Vines, S. K. (2021). Impacts of ionospheric ions on magnetic reconnection and earth's magnetosphere dynamics. *Reviews of Geophysics*, *59*(3), e2020RG000707. https://doi.org/10.1029/2020RG000707

Torbert, R. B., Burch, J. L., Phan, T. D., Hesse, M., Argall, M. R., Shuster, J., et al. (2018). Electron-scale dynamics of the diffusion region during symmetric magnetic reconnection in space. *Science*, *362*(6421), 1391–1395. https://doi.org/10.1126/science.aat2998

Ugai, M. (1984). Self-consistent development of fast magnetic reconnection with anomalous plasma resistivity. *Plasma Physics and Controlled Fusion*, *26*(12B), 1549–1563. https://doi.org/10.1088/0741-3335/26/12b/010

Ugai, M., & Tsuda, T. (1977). Magnetic field-line reconnexion by localized enhancement of resistivity: Part 1. Evolution in a compressible mhd fluid. *Journal of Plasma Physics*, *17*(3), 337–356. https://doi.org/10.1017/S0022377800020663

Yan, M., Lee, L. C., & Priest, E. R. (1993). Magnetic reconnection with large separatrix angles. *Journal of Geophysical Research*, *98*(A5), 7593–7602. https://doi.org/10.1029/92ja02644

Zelenyi, L., Malova, H., & Popov, V. (2003). Splitting of thin current sheets in the earth's magnetosphere. *JETP Letters*, *78*, 296–299. https://doi.org/10.1134/1.1625728

Zenitani, S., Hesse, M., & Klimas, A. (2009). Two-fluid magnetohydrodynamic simulations of relativistic magnetic reconnection. *The Astrophysical Journal*, *696*(2), 1385–1401. https://doi.org/10.1088/0004-637x/696/2/1385

Zweibel, E. G., & Yamada, M. (2009). Magnetic reconnection in astrophysical and laboratory plasmas. *Annual Review of Astronomy and Astrophysics*, *47*(1), 291–332. https://doi.org/10.1146/annurev-astro-082708-101726